Pore Diffusion Simulation Model of Bimodal Catalyst for Fischer-Tropsch Synthesis

Bolian Xu and Yining Fan
Laboratory of Mesoscopic Materials Science, Dept. of Chemistry, Nanjing University, Nanjing 210093, China

Yi Zhang and Noritatsu Tsubaki
Dept. of Applied Chemistry, School of Engineering, Toyama University, Gofuku 3190, Toyama 930-8555, Japan

DOI 10.1002/aic.10469
Published online May 16, 2005 in Wiley InterScience (www.interscience.wiley.com).

The Fischer-Tropsch (FT) synthesis reaction was conducted using bimodal catalyst in a slurry phase reactor. The bimodal catalyst was prepared from a bimodal support which was tailor-made by introducing SiO_2 sol directly into the large pores of a SiO_2 gel pellet The bimodal catalyst exhibited significantly higher activity in the slurry-phase Fischer-Tropsch synthesis than in other unimodal catalysts. The support with a large surface area allowed a highly dispersed cobalt particle, and its large pore size improved the diffusion of reactants and products. The diffusion of reactants inside the catalyst pores was simulated, and the effects of pore structure and pore size on catalytic performances were consistent with the simulation results. © 2005 American Institute of Chemical Engineers *AIChE J,* 51: 2068–2076, 2005

Keywords: Fischer-Tropsch synthesis, bimodal, diffusion, simulation, cobalt catalyst.

Introduction

From the energy crisis in the early 1970s, FT synthesis process was paid much attention, especially when more natural gas resources were found in the world. Recently, many works were conducted on the liquid-phase and super-critical phase Fischer-Tropsch synthesis (FTS) reaction, because of the advantages in temperature control, wax extraction and catalyst lifetime extension.[1-2] However, the main drawback of the liquid-phase FTS reaction was the slow diffusion rate of the syngas and products inside the pores which filled with formed hydrocarbons and solvent.[3-4] A good catalyst for liquid-phase FTS reaction must be with large pores to reduce the pore diffusion resistance. On the other hand, the large surface area of catalyst support is favorable to increase metal dispersion, leading to high CO conversion of the supported FT metal catalysts. Unfortunately, a higher surface area means a smaller pore size, and the stronger pore resistance. Furthermore, the shape and size of the pore can affect the reaction pathways.[5-6] Until now, few preparation methods of bimodal catalyst support were developed. Furthermore, all reported methods were only useful for one kind of oxide support. For example, the preparation method of alumina bimodal catalyst support cannot be applied to silica bimodal support. A generous preparation method is necessary to develop. Moreover, in most cases, strong acid base and organic solvents were used in the previous methods. The size of a large pore in bimodal catalyst support prepared by the previous method was too big, such as 100 nm to 500 nm, thus, lowering the effect of bimodal structure. A simple bimodal catalyst supported preparation method using safe solvent, which can precisely control pore size, is of great importance. Inui et al. developed a kind of bimodal Ni/SiO_2 catalyst, utilizing very strong acidic corrosion function of *aqua regia.*[7] It showed high activity for methantion of CO_2. The bimodal catalyst, where both large pore and small pore coexist, can guarantee high-transport efficiency, because the large pores lead to a high-diffusion rate of reactants and products, while the small pores lead to a large surface area, and finally a high-metal surface area in the supported metal catalyst.

Practically, slurry-phase FTS reaction has the problem of

Correspondence concerning this article should be addressed to N. Tsubaki at tsubaki@eng.toyama-u.ac.jp

wax accumulation in slurry, especially in long-time reaction, resulting in high viscosity, rising up of slurry level in the reactor, and slow diffusion rate in the bulk slurry. To avoid this problem, on-line wax release from slurry through a filter is necessary. A catalyst pellet with small enough size is favorable for slurry-phase FTS reaction, due to its high catalyst effectiveness factor, but is not suitable for wax filter as small catalyst powder can pass through the filter, leading to catalyst loss and product contamination. On this meaning, bimodal catalyst pellet with suitable size (not too small) is important to keep the wax filter working well, while the catalyst effectiveness factor is still high.

Here, we developed a new, safe and simple method to prepare bimodal catalyst support using nanoparticles in sol. The promotion role of the bimodal catalyst was investigated by liquid-phase FTS reaction. In this work, we also used a mathematical model to discuss the reactant diffusion behavior inside the pores in different catalyst, especially in bimodal catalyst. The diffusion effect on slurry-phase FTS reaction was also investigated.

Experimental

Catalyst preparation

The bimodal support was prepared by incipient-wetness impregnation of commercially available silica gel (Cariact Q-50, Fuji Silysia Co., specific surface area: 70 $m^2 \cdot g^{-1}$, pore volume: 1 $mL \cdot g^{-1}$, pellet size: 74–590 μm, and pore dia. 50 nm) with silica sol (Snowtex XS, Nissan Chemicals Co., aqueous solution, 20 wt %, SiO_2 particle size 5nm.) of a different concentration. After the impregnation, the support was dried in air at 393 K for 12 h, and then calcined in air at 673 K for 2 h. The loading of silica from snowtex sol was 11.2%, which was calculated from the weight increment after impregnation and calcination. Some silica support, which was noted as contrast silica support, was prepared from the silica sol above only at the same drying and calcining condition (air atmosphere, 393 K for 12 h, and 673 K for 2h) without impregnation into the large-pore silica.

Supported cobalt catalyst with 10 wt % metal loading was prepared by incipient-wetness impregnation of different supports, including the bimodal support, with cobalt nitrate aqueous solution. The catalyst precursors were dried in air at 393 K for 12 h, then calcined in air from room-temperature to 673 K with a ramping rate of 2 $K \cdot min^{-1}$, and kept at 673K for 2 h. After calcination, the catalysts were reduced in flowing hydrogen at 673 K for 10 h, and at last, passivated by 1% oxygen in nitrogen.

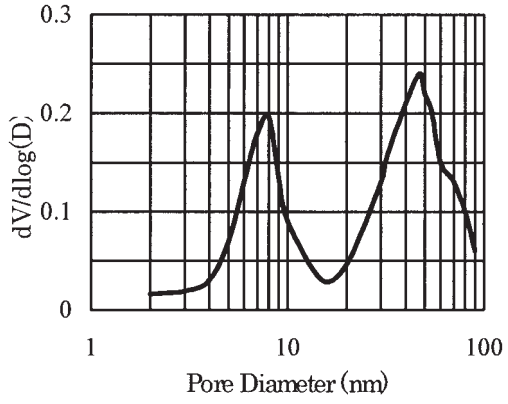

Figure 1. Pore-size distributions of bimodal catalyst.

Table 1. The Properties of Various Supports

Support	Surface Area m^2/g	Pore Volume ml/g	Pore Size nm
Q-50	70	1.0	50
Bimodal	106	0.46	6.0, 45
Q-3	546	0.3	3.0

Reaction and analysis

FTS reaction was carried out in a semibatch autoclave with the inner volume of 80 mL. The agitation speed of the stirrer was 2,000 rpm, which was carefully checked to eliminate diffusion-controlled possibility. The passivated catalyst (1.0g, under 149 μm) and 20 mL liquid medium, *n*-hexadecane, were loaded in the reactor. During the reaction, effluent gas released from the reactor was analyzed by on-line gas chromatography. CO and CO_2 were analyzed by using an active charcoal column equipped with a thermal conductivity detector (TCD). The hydrocarbons were also analyzed on-line using columns for $C_1 - C_5$ (Porapak Q), and for $C_6 - C_{20}$ (SE-30, uniport), respectively. The carbon balance was between 95 and 98% for all of reactions. Argon was employed as an internal standard with concentration of 3% in the feed gas. The reaction conditions were P (total) = 1.0 MPa, CO/H_2 = 1/2, W/F (CO + H_2 + Ar) = 10 $g \cdot h \cdot mol^{-1}$, T = 513 K.

Pore-size distribution, BET surface area and pore volume, were determined by the measuring instrument for surface area and pore size of porous materials (Shimadzu ASAP 2000), where nitrogen was used as absorbent. The metal surface area (metal dispersion) was determined by the same instrument via chemical adsorption mode using H_2 as absorber. Supported cobalt crystalline size was detected by TEM (TOPCON EM-002B, acc.volt: 200 kV, point resolution: 0.18 nm, line resolution: 0.14 nm).

Software for simulation

The differential equations of simulation were solved with a computational software (EQUATRAN®;-G all-purpose equation solver for windows, Version 3.0.1, Omega Simulation Co., Ltd.).

Results and Discussion

Physical structures of the Co/SiO_2 catalysts

Figure 1 showed the pore distribution of the bimodal catalyst prepared from the bimodal support. The physical properties of all support before impregnation are shown in Table 1. It gave clear evidence that two kinds of pore existed. The two-pore diameters of bimodal catalyst prepared from snowtex XS were 8 and 47 nm, respectively. 47 nm-pore was from the intrinsic pore of the used cariact Q-50 pellet, and 8 nm-pore was the new pores formed from 5 nm SiO_2 particle in silica sol snowtex. From the pore distribution of the bimodal catalyst, the pore volume of the large pore and small pore in the catalyst were 0.186 mL/g and 0.094 mL/g, respectively. Furthermore, the

Table 2. The Properties of Co/SiO_2 Catalyst* Derived from Various Supports

Catalyst	Surface Area m^2/g	Pore Vol. ml/g	Pore Size nm	Metal Surface Area m^2/g	TEM Crystal Size nm
Q-50 catalyst	52	0.82	54.0	1.724	37
Bimodal catalyst	82	0.28**	8.0; 47.0	0.701	22.6
Q-3 catalyst	513	0.16	3.7	1.964	1.4

* Cobalt loading: 10%.
**Large-pore volume was 0.186 ml/g, and the small-pore volume was 0.094 ml/g.

pore volume of bimodal support was 0.46 mL/g, while that as a contrast, silica support was 0.30 mL/g. If the loading silica was physically mixed with Cariact Q-50 pellet, the pore volume would be 1.0*88.8%+0.30 *11.2% = 0.92 mL/g as 11.2% weight was from nanopariticles in sol, shown in the catalyst preparation. The smaller real value, 0.46 mL/g, suggested that snowtex sol indeed entered the pores in Q-50 supports. The properties of Co/SiO_2 catalyst derived from various supports were shown in Table 2. Q-3 is a kind of SiO_2 support with a pore size of 3 nm. Catalyst prepared from Q-3 support had the largest surface area, but the smallest pore dia., and the catalyst prepared from Q-50 support had the lowest surface area and the largest pore size. The catalyst prepared from bimodal support had a moderate surface area and two kinds of pores. The TEM data showed the mean supported cobalt crystalline size as 37 nm for Q-50 catalyst, 22.6 nm for bimodal catalyst, and 1.4 nm for Q-3 catalyst. The mean cobalt particle size increased with increasing pore size. A small pore size support led to a small cobalt particle. However, for the metallic cobalt surface area, both the particle size and the reduction degree of cobalt can affect it. Consequently, it did not give a clear relationship with the pore size.

The reaction behavior of the Co/SiO_2 catalysts

The reaction performance of the catalysts prepared from the bimodal support or Q-50, Q-3 was compared in Table 3. The reaction rate of all catalysts reached steady state at 1 h from reaction start. Q-3 was an analogy to Q-50, but with an average pore size of 3 nm. Catalyst prepared from Q-3 support had the largest surface area, but the smallest pore diameter. It exhibited normal catalytic activity, but high methane selectivity. For the catalyst prepared from Q-50 support, which had the lowest surface area and the largest pore size, the CO conversion was the lowest. For the catalyst prepared from bimodal support, the CO conversion was the highest, and, meanwhile, selectivities of CH_4 and CO_2 were as low as to those of the catalyst prepared from Q-50. Bimodal catalyst showed the best performances here.

The activities and selectivities of the FTS catalysts were markedly depending on their pore structure. The catalyst having a small pore size tended to produce lighter hydrocarbons. On the other hand, the product distribution of large pore catalyst was wider, and the proportion of the heavy hydrocarbon was higher.[8] It has been already pointed out that the propagation of the carbon-carbon chain occurred more easily on the catalyst with lower specific surface area where metallic particle size was larger,[9-10] which naturally decreased methane formation. Furthermore, 1-olefins are generally produced as primary products in FTS, and are successively hydrogenated to paraffin.[11] However, they can readsorb onto metallic sites to receive secondary hydrocracking, breaking the terminal double-bond and releasing methane, especially in the liquid-phase FTS reaction. When the pore size was larger, the transportation of the primary product was more effective and relevantly methane formation rate from secondary hydrocracking of olefins was lower. Also lower BET surface area of large pore support determined larger metallic size and suppressed methane formation. On the basis of these reasons, the methane selectivity was the lowest for the catalyst prepared from Q-50. Due to the larger pore existing in the catalyst prepared from bimodal support, the CH_4 selectivity was also low. On the other hand, FT synthesis rates on cobalt catalyst can be improved by increasing the dispersion of supported cobalt crystalline. Generally, the metal dispersion is increased with the increasing surface area, and decreasing of pore size of support. For Q-3 derived catalyst, its small pore and slow diffusion efficiency determined high methane selectivity. However, its CO conversion was not the highest, regardless of its highest metal dispersion in this study.

Table 3. The Reaction Performance of Cobalt Catalysts Prepared from Different Supports

Catalyst	Q-50	Bimodal	Q-3
CO conv. (%)	11.8	32	16.9
Methane sel. (%)	7.1	8.2	35.8
CO2 sel. (%)	3.2	2.8	33
Chain growth probability	0.86	0.86	0.84

Reaction conditions: 513 K, 1.0 MPa, W/F = 10 g · h · mol^{-1}, H_2/CO = 2, cobalt loading: 10 wt%.

The BET surface area and pore volume decreased and average pore size increased very slightly for various Co/SiO_2 catalysts after cobalt loading, compared to the original supports, since the supported cobalt crystalline blocked some smaller pores of support. However, the bimodal catalyst still kept bimodal structure with two kinds of pore size of 8nm and 47 nm, as shown in Figure 1. Bimodal catalyst, having higher metal dispersion due to its larger BET surface area, and an accelerated diffusion rate derived from the bimodal structure, exhibited the highest CO conversion and low methane selectivity. The chain growth probability was calculated from the product weight distribution by neglecting irregular $C_1 - C_3$, because of the strong secondary reactions in liquid phase.[12] The chain growth probability did not change significantly. It was 0.86, 0.86 and 0.84 of the catalysts derived from Q-50, bimodal, and Q-3, respectively. The chain growth probability can be affected by many factors, such as pore resistance time,[6] metal particle size,[9] H_2/CO ratio and catalyst pellet size.[11] Small metal particles lower chain growth probability, but slow diffusion rates of hydrocarbons inside pores increase it. Maybe the combination of many factors leads a slight change in the chain growth probability for Q-3 catalyst.

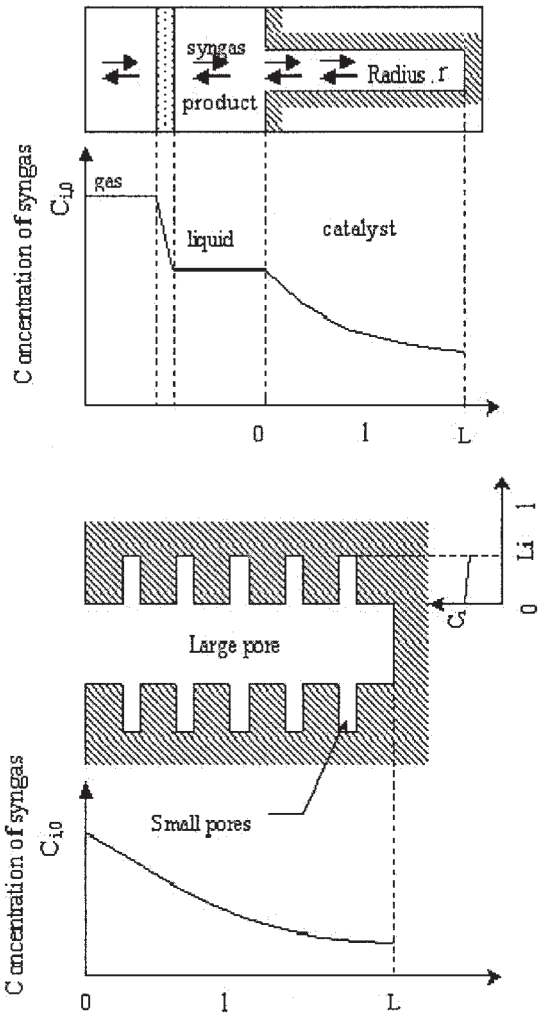

Figure 2. Unimodal or bimodal porous structure with one or two size's of pores as a model for different catalyst.

Simulation of diffusion of reactants and the effectiveness factor of the catalyst in the slurry reaction

Mathematical model. A theoretical explanation is attempted in this section for the experimental results presented earlier. In Figure 2, the model is shown. Supposing the Q-50 and Q-3 catalysts with single cylindrical pores with inner radius r and depth L, reactants dissolved in the solvent through the liquid boundary layer. They moved in the bulk liquid that was agitated mechanically to reach the outer surface of the catalyst particle. They finally diffused into the pores, from pore mouths, which were filled with liquid media and reach the inner surface of catalyst particle, where the active component Co metal was dispersed. The relationship between rate constants on different bases is given by

$$k_V \cdot \pi r^2 \cdot L = k_S \cdot 2\pi r \cdot L; \quad k_V = \frac{2k_S}{r} \tag{1}$$

where k_V is the reaction rate constant based on pore volume, while k_S on surface area; r is the pore radius.

Generally, FT reaction kinetics has been represented by a power rate law, and the rate can be shown by the following equation

$$v = k_V C_{H_2}^x C_{CO}^y = \frac{2k_S}{r} C_{H_2}^x C_{CO}^y \tag{2}$$

where x and y are the exponential dependencies on H_2 and CO concentration.

For bimodal catalyst, the little pore is not so deep that diffusion effect in the small pores can be neglected. Consequently, the small pores just increase the total surface area. The diffusion in large pores was only considered here, and the diffusion effect in small pores will be proved to be negligible in the *Simulation results* section. If the diffusion in large pores is onlyconsidered, the suppositional reaction constant based on large pore surface area (k_S^*) should be introduced for simulation.

$$k_S \cdot S_{total} = k_S^* \cdot S_L; \quad k_S^* = k_S \frac{S_{total}}{S_L} \tag{3}$$

where k_S is on the support total surface area, but k_S^* is on large pore surface area; S_L is the surface area of the large pores. S_L can be calculated from the large pore volume V_L, and large pore radius r

$$S_L = \frac{2V_L}{r} = \frac{2 \times 0.186 \times 1000}{47/2} = 15.83 m^2/g \tag{4}$$

The same as Eq. 1, the suppositional reaction constant based on large pore volume (k_V^*) can be expressed as

$$k_V^* = \frac{2k_S^*}{r} = \frac{2k_S}{r} \frac{S_{total}}{S_L} \tag{5}$$

Thus, the reaction rate in bimodal catalyst can be expressed as

$$v = k_V^* C_{H_2}^x C_{CO}^y = \frac{2k_S^*}{r} C_{H_2}^x C_{CO}^y = \frac{2k_S}{r} \frac{S_{total}}{S_L} C_{H_2}^x C_{CO}^y \tag{6}$$

In fact, the reaction was performed on the surface of the metal particles, if the reaction rate constant based on the metal surface area; Eq. 2 should be changed to

$$v = k_V C_{H_2}^x C_{CO}^y = \frac{2k_{Co}}{r} \frac{S_{Co}}{S_{total}} C_{H_2}^x C_{CO}^y \tag{7}$$

where k_{Co} is the reaction rate constant, based on the metal surface area; S_{Co} and S_{total} are the surface area of metal cobalt and the total BET surface area. This equation gives the relationship between reaction rate constant based on specific metal surface area (k_{Co}), and reaction rate based on pore volume (k_V) in a cylinder pore.

For bimodal catalyst, it should be

$$v = k_V^* C_{H_2}^x C_{CO}^y = \frac{2k_{Co}}{r}\frac{S_{total}}{S_L}\frac{S_{Co}}{S_{total}} C_{H_2}^x C_{CO}^y = \frac{2k_{Co}}{r}\frac{S_{Co}}{S_L} C_{H_2}^x C_{CO}^y \quad (8)$$

In the slurry reaction, the influence of reactant diffusion in the liquid laminar can be neglected due to rapid agitating. Thus, the reactant, CO and H_2 concentration at the entrance of the pore would be the same as the concentration in the bulk solution. On the basis of the second Fick's Law

$$D_{H_2}\frac{d^2C_{H_2}}{dl^2} = v_{H_2} \quad (9)$$

$$D_{CO}\frac{d^2C_{CO}}{dl^2} = v_{CO} \quad (10)$$

where D_{H2} and D_{CO} are the effective diffusion coefficients for hydrogen and carbon monoxide in the pore, respectively; l is the position in the pore; v_{H2} and v_{CO} is the reaction rate per unit pore volume for H_2 or CO; and C_{H2} and C_{CO} are the concentrations of reactants.

The boundary conditions are

$$C_{H_2} = C_{H_2,0}, \quad C_{CO} = C_{CO,0}, \quad \text{at } l = 0 \quad (11)$$

$$\frac{dC_{H_2}}{dl} = \frac{dC_{CO}}{dl} = 0, \quad \text{at } l = L \quad (12)$$

In Eqs. 2 and 6, the reaction rate can be expressed as

$$v = v_{CO} = \frac{1}{2}v_{H_2} = k_V C_{H_2}^x C_{CO}^y \quad (13)$$

where k_V is the rate constant; x and y are the exponential dependencies on H_2 and CO concentration.

Furthermore, the rate equation for this system was determined experimentally. In the experiment, finely-crushed Q-50 catalyst was tested in slurry phase reaction to eliminate the most possible diffusion influence. At first, Q-50 catalyst with large pore only was tested for varied composition of syngas where partial pressure of H_2 was changed and partial pressure of CO was fixed. In order to keep the total pressure the same, N_2 was used as the balanced gas. It was found that dependency of H_2 was first-order. The following relationship was available

$$v = kC_{H_2}f(C_{CO}); \quad v/C_{H_2} = kf(C_{CO}) \quad (14)$$

where k is the apparent reaction constant; $f(C_{CO})$ is the function of CO concentration in liquid.

Testing syngas with different composition, the relationship between $V/(C_{H2})$ and C_{CO} was obtained, as exhibited in Figure 3. From this figure, expression of the function $kf(C_{CO})$ was decided using best fitting equation

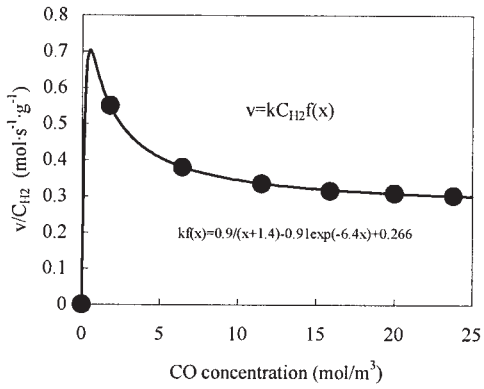

Figure 3. Reaction rate as a function of CO concentration.

Reaction conditions: 513 K, 1.0 MPa, W/F = 10 g·h·mol^{-1}

$$\frac{kf(C_{CO})}{\text{mol}\cdot\text{s}^{-1}\cdot\text{g}^{-1}} = \frac{0.90}{\dfrac{C_{CO}}{\text{mol}\cdot\text{m}^{-3}} + 1.4} - 0.91\exp\left(\frac{-6.4C_{CO}}{\text{mol}\cdot\text{m}^{-3}}\right) + 0.266 \quad (15)$$

It is found that the reaction rate tended to constant when CO concentration is high. It indicated that the dependency of CO concentration was zero-order in high CO concentration condition. So the limitation of the function $f(C_{CO})$ should be 1. The apparent reaction constant was 0.266 m^3·g^{-1}·s^{-1}. Thus, the expression of function $f(C_{CO})$ was

$$f(C_{CO}) = \frac{3.38}{\dfrac{C_{CO}}{\text{mol}\cdot\text{m}^{-3}} + 1.4} - 3.42\exp\left(\frac{-6.4C_{CO}}{\text{mol}\cdot\text{m}^{-3}}\right) + 1.00 \quad (16)$$

The catalyst effectiveness factor η was defined to measure how much the reaction rate is lowered because of the resistance to pore diffusion, as follows

$$\eta = \frac{(\textit{actual reaction rate within pore})}{(\textit{rate if not slowed by pore diffusion})} = \frac{\bar{v}_{\textit{with diffusion}}}{v_{\textit{without diffusion}}} \quad (17)$$

From the CO or H_2 diffusion speed at the entrance of the pore and the ideal expression of the reaction rate, the effectiveness factor can be expressed as

$$\eta = \frac{-D_{CO}\left(\dfrac{dC_{CO}}{dl}\right)_{l=0}\pi r^2}{k_V C_{H_2,0} f(C_{CO,0})\pi r^2 L} = \frac{-D_{CO}\left(\dfrac{dC_{CO}}{dl}\right)_{l=0}}{k_V C_{H_2,0} f(C_{CO,0}) L} = \frac{-D_{H_2}\left(\dfrac{dC_{H_2}}{dl}\right)_{l=0}\pi r^2}{2k_V C_{H_2,0} f(C_{CO,0})\pi r^2 L} = \frac{-D_{H_2}\left(\dfrac{dC_{H_2}}{dl}\right)_{l=0}}{2k_V C_{H_2,0} f(C_{CO,0}) L} \quad (18)$$

From the CO converting rate in pores $k_V\eta C_{H_{2,0}} f(C_{co,0})$, and the specific pore volume V, the CO reaction rate on the unit weight catalyst can be expressed as $k_V\eta C_{H_2,0} f(C_{co,0})V$. It should be noticed that the unit of CO converting rate in pores is mol·m^{-3}·s^{-1}, but the CO reaction rate on unit weight catalyst $k_V\eta C_{H_{2,0}} f(C_{co,0})$V is mol·g^{-1}·s^{-1}. On the other hand, CO flow rate on the unit weight of catalyst is $(F/W)_{CO}$, so the CO conversion can be expressed as

$$conv. = \frac{k_V\eta C_{H_{2,0}} f(C_{co,0})V}{(F/W)_{CO}} \tag{19}$$

where V is the pore volume of the catalysts, and F/W is the reactant flow rate for the unit weight of the catalyst.

Calculation of the diffusion coefficient and other parameters

Although, the detection of the diffusion coefficient for molecules in a solvent is very difficult, it is practical to apply the Stokes-Einstein method in hydrodynamics, as well as the experiment verification

$$D = \frac{K_B T}{6\pi a f} \tag{20}$$

where D is the diffusion coefficient of a Brownian sphere of radius a in a continuum with viscosity f and temperature T, when no slip exists between the particle and the continuum. K_B is the Boltzmann constant. In Fischer-Tropsch synthesis, it is considered that the pores in catalyst are filled with high-boiling wax. In our calculation, we use the viscosity of FT wax at the experiment temperature (2.45 mPa·s, from the Shell Company.).

The molecular diffusion coefficient obtained earlier does not consider the pore size effect. In gas-phase diffusion, there is a Wheeler equation to describe the diffusion coefficient in small pores[13]

$$D = \frac{1}{3}\bar{u}\lambda(1 - e^{-2r/\lambda}) \tag{21}$$

where $\bar{u}$ is the mean speed of the gas molecule, λ is the mean free path, and r is the radius of the pore. In fact, the first part of the Eq. 21, $(1/3)\bar{u}\lambda$, is the diffusion coefficient without pore size effect in gas-phase diffusion,[14] so the second part, $1 - e^{-2r/\lambda}$, can be deemed to the pore size effect factor. It is referred that the hydrogen or carbon monoxide molecule in solvent follows the Brownian motion, and it is able to suppose that the hydrogen or carbon monoxide molecule was in a "viscous space". So the mean free path of hydrogen can be expressed as follows[15]

$$\lambda = \frac{1}{\sqrt{2}\ \pi d^2(P/K_B T)} = \frac{1}{\sqrt{2}\ \pi d^2 N_A C_{H_{2,0}}} \tag{22}$$

where d is the molecule diameter; P is pressure; K_B is Boltzman constant; T is temperature; N_A is the Avogadro constant and $C_{H2,0}$ is the concentration of hydrogen in solvent.

As a result, the real diffusion coefficient in pores can be derived as

$$D_e = D(1 - e^{-2r/\lambda}) \tag{23}$$

Supposing the solubility of H_2 and CO in the solvent follow the Henry's Law, and we get the Henry coefficient from literature.[16] Then the solubilities of H_2 and CO in the solvent (cetane) can be calculated to be 46.6 and 23.8 mol/m^3 in the reaction condition.

For porous catalyst pellet, the proper measure of pore depth could be expressed as follow[17]

$$L = \frac{volume\ of\ pellet}{exterior\ surface\ available\ for\ reactant\ penetration\ and\ diffusion}$$

and for spherical pellet, $L = 3/R$, where R is the catalyst pellet radius.

In this experiment, the catalysts we used were sieved at 80–100 mesh, and the pellet radius was about 75 μm. The depth of the pore would be 25 μm.

All the parameters for simulation are shown in Table 4.

Simulation results

From Eqs. 18 and 19, the dC_{CO}/dL and dC_{H2}/dL at l = 0 can be calculated.

$$\left(\frac{dC_{CO}}{dl}\right)_{l=0} = \frac{-k_V C_{H_{2,0}} f(C_{CO,0})L}{D_{CO}} = -\frac{conv. \times (F/W)_{CO} L}{D_{CO} \times V}$$

Table 4. The Parameters for Simulation and Some Simulation Results

Catalyst	Q-50	Q-3	Bimodal
Pore size (nm)	54	3.7	8.0; 47
Co particle size (nm)	37	1.4	22.6
Conv. (%)	11.8	16.9	32
D_{H2} (10^{-10} m^2/s)	4.74	0.434	4.28
D_{CO} (10^{-10} m^2/s)	3.38	0.308	3.05
$C_{H2,0}$ (mol/m^3)	46.6	46.6	46.6
$C_{CO,0}$ (mol/m^3)	23.8	23.8	23.8
L (10^{-5} m)	2.5	2.5	2.5
k_V (k_V^* for bimodal catalyst) (s^{-1})	0.0258	1.094	0.403
k_{Co} (10^{-8} m/s)	1.05	74.1	3.81
Catalyst Effective Factor η	0.98	0.17	0.75

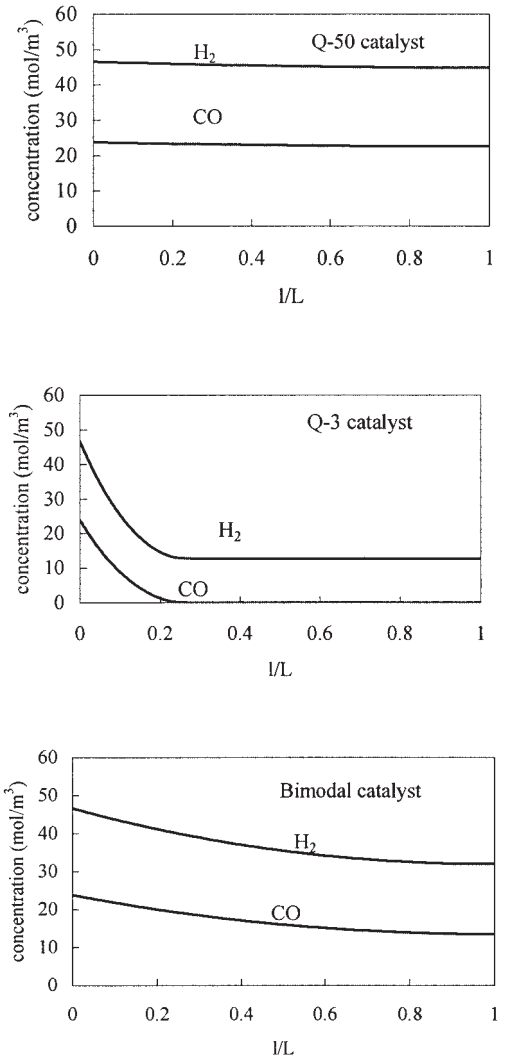

Figure 4. Simulation of the effect of catalyst pore size on the reactant concentration profiles inside the pores.

$$\left(\frac{dC_{H_2}}{dl}\right)_{l=0} = \frac{-2k_V C_{H_2,0} f(C_{CO,0})\, L}{D_{H_2}} = -\frac{2 \times conv. \times (F/W)_{CO} L}{D_{H_2} \times V}$$

They and the reactants concentration ($C_{CO,0}$ and $C_{H2,0}$) were set as initial value in simulating Eqs. 24 and 25 by computational software (EQUATRAN®-G).

$$D_{H_2} \frac{d^2 C_{H_2}}{dl^2} = 2k_V C_{H_2} f(C_{CO}) \tag{24}$$

$$D_{CO} \frac{d^2 C_{CO}}{dl^2} = k_V C_{H_2} f(C_{CO}) \tag{25}$$

In the simulation, the pore depth L was divided to 1,000 segments. On a given k_V or k_V^*, the program gave a series of C_{CO}, C_{H2}, dC_{CO}/dL and dC_{H2}/dL. Different k_V or k_V^* was tested until the simulated dC_{CO}/dL and dC_{H2}/dL values fit the boundary condition (Eq. 12). Consequently, the metal surface kinetic constant k_{Co} was calculated by Eqs.7 and 8.

The reactants concentration profiles inside pores are shown in Figure 4. Obviously, the concentration profiles of reactants inside the pores in Q-50 and bimodal catalyst were changed slightly. However, in Q-3 catalyst, it decreased quickly. It suggests that the pore diffusion resistance in the bimodal catalyst is not strong. From the profile of reactant concentration distribution, it can be easily found that in Q-3, the CO concentration will decrease to 0 in pores when $l/L > 0.22$. That must be another reason it caused a higher CH_4 selectivity[18].

In Table 4, some other simulation results are compared. First, the explanation for neglecting the inner pore diffusion in small pores of bimodal catalyst will be given. The large pore size of bimodal catalyst (47 nm) is 7 nm smaller than the Q-50 catalyst (54 nm), due to the fact that nanoparticles formed the small pores on the wall of the original Q-50 pores. So the mean depth of small pores is about 3.5 nm. From Eqs. 20 – 23, the diffusion coefficient in the small pore for H_2 and CO are calculated about $6.68*10^{-11}$ $m^2 \cdot s^{-1}$, and $3.33*10^{-11}$ $m^2 \cdot s^{-1}$, respectively. The metal surface reaction kinetic constant k_{Co} in bimodal catalyst is $3.81*10^{-8}$ $m \cdot s^{-1}$. From the relationship of the kinetic constant, based on surface area, and the kinetic constant, based on pore volume in cylinder pores, described as Eq. 7, the reaction kinetic constant k_V in small pores is 0.521 s^{-1}. With the same method, the reactants diffusion action was simulated by EQUATRAN®-G. The catalyst effectiveness factor η is very close to 1 (0.999996) in these small pores. The reactants concentration distribution inside the small pores was shown in Figure 5. It indicates that the supposing of neglecting the inner-pore diffusion is reasonable.

The reaction rate based on specific metal surface k_{Co} increased with the decreasing of metal particle size. It is easy to know that the metal particle size depends on pore size support. For bimodal catalyst, there are some small cobalt particles in small pores while some large particles in large pores. The small cobalt particles reaction rate is high as the Q-3 catalyst, while the large cobalt particle is normal as Q-50 catalyst. There is almost no pore diffusion resistance in small pores in bimodal catalyst as discussed earlier. These lead to a moderate average reaction rate for bimodal catalyst. The catalyst effectiveness factors of Q-50, Q-3, and bimodal catalysts are 0.98, 0.17 and 0.75, respectively. It also means that there is almost no pore diffusion resistance in Q-50 catalyst, while a strong pore diffusion resistance in Q-3 catalyst. Also, the pore diffusion resistance in bimodal catalyst is not important. The apparent

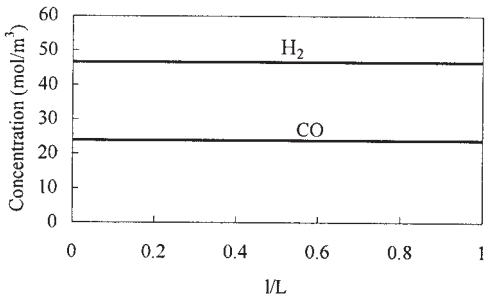

Figure 5. Reactant concentration profiles inside the small pores in bimodal catalyst.

Table 5. The Apparent Activation Energy of FTS Reaction in Different Catalyst

Catalyst	Q-50	Q-3	Bimodal
$\Delta \ln(\text{conv.})/\Delta(1/T)$ (K)	13409.4	7237.7	9387.8
Activation energy (kJ/mol)	111.5	60.2	78.0

activation energies estimated from the CO conversions between 513 K and 533 K were shown in Table 5. As proven elsewhere, in strong pore diffusion resistance catalyst, the apparent activation energy of the reaction is about half of the intrinsic value.[19] The apparent activation energy of Q-50 without pore diffusion resistance is 111.5kJ/mol. This value is about twice of the activation energy of Q-3 with a strong pore diffusion resistance. Also, the moderate activation energy of bimodal catalyst suggests that the pore diffusion resistance is not very strong.

It is clear that building up silica bimodal catalysts realize the spatial promotion of the reaction. It improves the diffusion rate of syngas and products, and the dispersion of active metal particles, respectively. These results indicate that a new, simple and general method for preparing bimodal support is developed by manipulation of silica nanoparticles from its sol inside the pores of silica gel. By this method, the bimodal support with both large pore of the desired size and micropore, can be easily prepared. In fact, it is also found by these authors that small pore size in this method was equal to the diameter of the nanoparticles in the sol.[20-21] Both large pore size and small pore size can be controlled precisely by this method.

Conclusion

A new, simple and safe preparation method was developed for bimodal catalyst support by manipulation of silica nanoparticles from its sol inside large pores of a silica gel. It had a large surface area and two kinds of pores tailor-made for reactant diffusion. This new kind of catalyst exhibited significantly higher activity in slurry-phase Fischer-Tropsch synthesis, than in other unimodal catalysts. Also, a mathematical model was developed to elucidate the kinetics coupled with mass transfer effect inside the pores of both unimodal and bimodal catalyst. In small pores, the smaller metal particle gave higher metal surface area and higher surface catalytic activity, but stronger reactant diffusion resistance. On the contrary, the large pore catalyst had lower surface activity, even without diffusion resistance. The obtained bimodal catalyst developed their good qualities, but avoided the defects as designed.

Notation

a = radius of Brownian sphere, m
C = concentration, mol·m^{-3}
d = molecule diameter, m
D = diffusion coefficient, m^2·s^{-1}
f = viscosity, kg·m^{-1}·s^{-1}
F = flow rate, mol·h^{-1}
k = apparent reaction constant, m^3·g^{-1}·s^{-1}
k_{Co} = reaction rate constant based on metal surface, m·s^{-1}
k_S = reaction rate constant based on support surface, m·s^{-1}
k_V = reaction rate constant based on support volume, s^{-1}
k_S^* = reaction rate constant based on large pores surface of support, m·s^{-1}
k_V^* = reaction rate constant based on large pores volume of support, s^{-1}
K_B = Boltzmann's constant, J·K^{-1}
l = position in the pore, m
L = depth of the pore, m
P = pressure, Pa
r = radius of the pore, m
R = radius of the particle, m
S = surface area, m^2·g^{-1}
T = temperature, K
u = molecule speed, m·s^{-1}
v = reaction rate, mol.m^{-3}·s^{-1}
V = pore volume, mL·g^{-1}
W = weight, g
x = exponential dependency
y = exponential dependency

Greek letters

η = effectiveness factor of catalyst
λ = mean free path, m

Subscripts

CO = carbon monoxide
Co = metal cobalt
H_2 = hydrogen
L = for large pore
S = for unit surface area
Total = silica support total surface area
V = for unit pore volume

Literature Cited

1. Fan L, Yokota K, Fujimoto K. Characterization of mass-transfer in supercritical-phase Fischer-Tropsch synthesis reaction. *Topics in Catalysis*. 1995;2:267-283.
2. Bochniak DJ, Subramaniam B. Fischer-Tropsch synthesis in near-critical n-hexane: pressure-tuning effects. *AIChE J.* 1998;44:1889-1896.
3. Post MFM, VantHoog AC, Minderhoud JK, Sie ST. Diffusion limitations in Fischer-Tropsch catalysts. *AIChE J*. 1989;35:1107-1114.
4. Fan L, Yokata K, Fujimoto K. Supercritical phase Fischer-Tropsch synthesis: Catalyst pore-size effect. *AIChE J*. 1992;38:1639-1649.
5. Schulz H. Spatial constraints and frustrated reactions in Fischer-Tropsch synthesis. *Catalysis Today.* 2003;84:67-70.
6. Iglesia E, Reyes SC, Madon RJ. Transport-enhanced alpha-olefin readsorption pathways in Ru-catalyzed hydrocarbon synthesis. *J Catal*. 1991;129:238-256.
7. Inui T, Funabiki M, Suehiro M, Sezume T. Methanation of CO_2 and CO on supported nickel-based composite catalysts. *J Chem Soc Faraday I.* 1979;75:787-802.
8. Sun S, Tsubaki N, Fujimoto K. Characteristic feature of Co/SiO_2 catalysts for slurry phase Fischer-Tropsch synthesis. *J Chem Eng Jpn.* 2000;33:232-238.
9. Nijs HH, Jacobs PA. Metal particle size distributions and Fischer-Tropsch selectivity: A extended Schulz-Flory model. *J Catal.* 1980; 65:328-334.
10. Fujimoto K, Nobusawa T, Fukushima T, Tominaga H. Activity and selectivity regulation of synthesis gas reaction over supported ruthenium catalyst. *Bull Chem Soc Jpn.* 1985;58:3164-3171.
11. Madon R, Reyes S, Iglesia E. Primary and secondary reaction pathways in ruthenium-catalyzed hydrocarbon synthesis. *J Phys Chem.* 1991;95:7795-7804.
12. Olive GH, Olive S. *The Chemistry of the Catalyzed Hydrogenation of Carbon Monoxide*. New York: Springer-Verlag; 1984:158
13. Wheeler A. Reaction rates and selectivity in catalyst pores. *Adv Catal.* 1951;3:249-275.
14. Atkins PW. *Physical Chemistry.* 3rd ed. Oxford: Oxford University Press; 1986:657.
15. Atkins PW. *Physical Chemistry.* 3rd ed. Oxford: Oxford University Press; 1986:653.
16. Breman BB, Beenackers AACM, Rietjens EWJ, Stege RJH. Gas-liquid solubilities of carbon monoxide, carbon dioxide, hydrogen, water, 1-alcohols ($1 \le n \le 6$), and n-paraffins ($2 \le n \le 6$) in hexadecane, ocatacosane, 1-hexadecanol, phenanthrene, and tetraethylene glycol at

pressure up to 5.5 MPa and temperatures form 293 to 553K. *J Chem Eng Data*. 1994;39:647-666.
17. Levenspiel O. *Chemical Reaction Engineering*, New York: Wiley; 1972:476.
18. Madon RJ, Iglesia E. Hydrogen and CO intrapellet diffusion effects in ruthenium-catalyzed hydrocarbon synthesis. *J Catal* 1994;149:428-437.
19. Levenspiel O. *Chemical Reaction Engineering*. New York: Wiley; 1972:491.
20. Zhang Y, Yoneyama Y, Tsubaki N. Bimodal porous silica prepared by pore-filling of silica Sol. *J Jpn Petroleum Inst*. 2003;46: 335-338.
21. Zhang Y, Shinoda M, Tsubaki N. Development of bimodal cobalt catalysts for Fischer-Tropsch synthesis. *Catalysis Today.* 2004;93:55-63.

Manuscript received Apr. 3, 2004, and revision received Nov. 11, 2004.